$$S = \frac{1}{\pi\epsilon}\int_{-\epsilon}^{\epsilon} \arcsin\left[\frac{\epsilon^2 - y^2}{A^2} - \frac{1}{4}\left(\frac{\epsilon^2 - y^2}{A^2}\right)^2\right]^{1/2} dy$$

$$\approx \frac{1}{\pi\epsilon}\int_{-\epsilon}^{\epsilon} \arcsin\left(\frac{\epsilon^2 - y^2}{A^2}\right)^{1/2} dy$$

$$\approx \frac{1}{\pi\epsilon A}\int_{-\epsilon}^{\epsilon} (\epsilon^2 - y^2)^{1/2}\, dy = \frac{1}{\pi\epsilon A}\cdot\tfrac{1}{2}\pi\epsilon^2 = \frac{\epsilon}{2A}.$$

Consequently,

$$\lim_{\epsilon\to 0} \frac{2(Aa)^{1/2}}{\epsilon}\int_0^{\infty} J_1(\epsilon x)J_0(ax)J_0(Ax)\, dx = \delta(A - a) \tag{A3}$$

and

$$g = \frac{1}{2A}\frac{\partial}{\partial A}[Av_1(A)] = \underline{\frac{1}{2}\left(v_1'(A) + \frac{v_1(A)}{A}\right)}. \tag{A4}$$

Therefore, the gain seen by the smaller carrier is given by the arithmetic mean of the slope of $v_1(a)$ and the large-signal gain $v_1(a)/a$ for $a = A$.

REFERENCES

[1] S. O. Rice, "Mathematical analysis of random noise," in *Selected Papers on Noise and Stochastic Processes*, N. Wax, Ed. New York: Dover, 1954.

[2] O. Shimbo, "Effects of intermodulation AM–PM conversion and additive noise in multicarrier TWT systems," *Proc. IEEE (Special Issue on Satellite Communications)*, vol. 59, pp. 230–238, Feb. 1971.

[3] E. Imboldi and G. R. Stette, "AM-to-PM conversion and intermodulation in nonlinear devices," *Proc. IEEE* (Lett.), vol. 61, pp. 796–797, June 1973.

[4] G. R. Stette, "Calculation of intermodulation from a single carrier amplitude characteristic," *IEEE Trans. Commun.* (Concise Papers), vol. COM-22, pp. 319–323, Mar. 1974.

[5] N. M. Blachman, "Detectors, bandpass nonlinearities, and their optimization: Inversion of the Chebeyshev transform," *IEEE Trans. Inform. Theory*, vol. IT-17, pp. 398–404, July 1971.

[6] D. Middelton, "The response of biased, saturated linear and quadratic rectifiers to random noise," *J. Appl. Phys.*, vol. 17, pp. 778–801, Oct. 1946.

[7] M. Abramowitz and I. A. Stegun, *Handbook of Mathematical Functions*. New York: Dover, 1965.

A Dynamic Calibration Method for Biphase Phase-Shift-Keyed Modulators

F. P. ZIOLKOWSKI, MEMBER, IEEE

Abstract—**A method is proposed whereby a (microwave) phase bridge can be constructed to *simultaneously* measure both the phase and amplitude balance of a biphase phase-shift-keyed (PSK) modulator. Given an initial *narrow-band* phase shifter that is capable of either continuous uncalibrated phase shifting or slow switching between calibrated fixed-90° phase shifts, the phase and amplitude balance of a second wide-band phase shifter (biphase modulator) can be determined. Furthermore, these measurements may be dynamically and simultaneously displayed in real time on a dual-trace oscilloscope. A significant feature of the method is the unique identification of either or both the phase and amplitude unbalance by means of the symmetric or asymmetric features that these unbalances induce in the display pattern.**

Quantitative criteria for the sensitivity of the technique are presented.

I. INTRODUCTION

THIS PAPER describes a scheme whereby a phase-bridge configuration can be used to characterize a RF phase-shift-keyed (PSK) biphase modulator for simultaneous phase and amplitude balance under dynamic conditions. The technique is applicable at any frequency where the basic bridge components are realizable, although the terminology used here is sometimes suggestive of waveguide.

Following this introductory section, Section II develops the two equations which describe the detected bridge voltages in terms of the modulator's phase and amplitude balance. Section II is therefore concerned with the appropriate representations for the phase bridge and the essential properties of components from which it is constructed. Given these results, Section III describes the waveforms that result when these voltages are displayed on a dual-trace oscilloscope. Five examples are described in detail with corresponding figures. The first example depicts the patterns for a perfectly balanced PSK modulator. The four remaining examples depict the patterns of special cases when the PSK modulator is slightly unblanced. Use of these latter four figures permits *any combination* of amplitude and phase unbalance of a PSK modulator to be readily identified in a quantitative manner. Section IV summarizes the salient features of the material developed in this paper.

Manuscript received December 1, 1973; revised June 1, 1974.
The author is with the Raytheon Company, Wayland, Mass. 01778.

II. THE REPRESENTATION OF THE DETECTED VOLTAGES

Fig. 1 depicts a phase bridge which is the basic configuration for the measurement technique. A CW signal from the source is divided between the two arms of the bridge, viz., the reference arm denoted I and the test arm denoted II. Although not shown explicitly in the figure, it is understood that sufficient isolation between the bridge arms must be maintained either by the use of isolators or padding, since in practice the hybrid junctions and particularly the diodes used in the detectors are not ideal. The components within each arm of the bridge may also require padding or isolation, since appreciable phase error can accrue if they are not matched.[1] In general, care consistent with good experimental procedure must be taken. The analysis, as given here, assumes that the single-ended detectors used are operated as square-law devices.

A. The Reference Arm

The reference arm of the bridge essentially contains a phase shifter and an attenuator. The properties of the reference-arm phase shifter utilized in this analysis are as follows.

1) Continuous uncalibrated variability from 0 to 360°, or alternatively, some form of arbitrarily slow switching between calibrated fixed-90° phase shifts that correspond to detected voltage nulls and maxima. In this latter case, the four required values are 0 to 90, 180, and −90°. In general, a continuously variable phase shifter is preferable since aligning the fixed phase shifts for precise nulls in effect requires some form of continuously variable phase shifter, although it need only be of limited range.

2) Attenuation invariance for all phase settings.

3) Adequate impedance match, although this can be corrected by sufficient padding if signal level is not a problem.

Furthermore, since this reference-arm phase shifter is modulated arbitrarily slowly (i.e., about 1 Hz or less as commensurate with visual pattern recognition) the signal is, for all practical purposes, CW. Therefore narrow-band components suffice. Examples of acceptable reference phase shifters are any that can be constructed using hybrids or circulators with mechanically variable sliding shorts, or electrically variable shorts with p-i-n diodes or ferrites. The rotary-vane phase shifter and the simple dielectric card phase shifter for waveguide operating in the TE_{10} mode are also acceptable, provided attention is given to the effects of attenuation variance as the phase is shifted. At lower UHF frequencies it becomes plausible to switch appropriate multiples of quarter-wavelength line in or out of the reference arm.

The requisite property of the reference-arm attenuator is to have sufficient attenuation range. Phase invariance with attenuation change is not important since the attenuation settings are not changed, as part of the method described here, once appropriate amplitude adjustments have been made. Appropriate impedance match is convenient although, as in the case of the phase shifter, this can be corrected by padding.

[1] This is a topic not amenable to concise pedagogical treatment, although it is unavoidably significant and important. Although by no means comprehensive, some relevant references are [1]–[3].

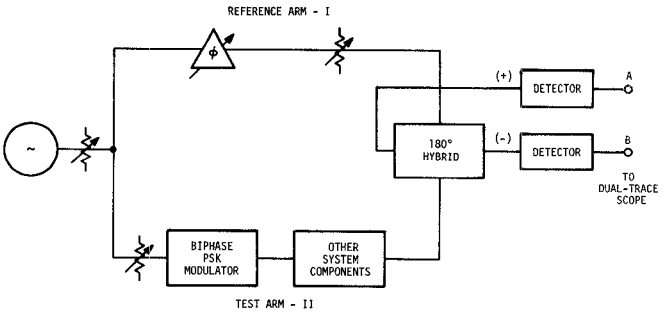

Fig. 1. Phase bridge for calibration of PSK modulator.

The signal from arm I at the input to the hybrid is represented by

$$V^{I}(t) = v^{I} \sin[wt + \phi_0]. \tag{1}$$

Strictly speaking, ϕ, the phase of arm I, is time dependent since the reference-arm phase is varied. However, as previously discussed, this variation is sufficiently slow to be represented by a constant ϕ_0 with negligible error. The quantity v^I is a constant.

B. The Test Arm

The test arm primarily contains the modulator under test, but may also include other components subsequently affecting system performance such as amplifiers, filters, etc. The modulator is assumed to be operating dynamically. Thus the signal from arm II at the input to the hybrid has the form

$$V^{II}(t) = v^{II}(t) \sin[wt + \theta(t)] \tag{2}$$

where

$$v^{II}(t) = v^{II}[1 \pm \Delta S(t)] \tag{3a}$$

$$\theta(t) = \theta_0 + \delta\theta S(t) \tag{3b}$$

$$\delta\theta = \pi \pm \epsilon. \tag{3c}$$

Here v^{II}, Δ, θ_0, $\delta\theta$, and ϵ are constants. The ideal biphase PSK modulator will have no amplitude unbalance ($\Delta = 0$) and no phase unbalance ($\epsilon = 0$ and $\delta\theta = \pi$). Any device that is useful as a modulator will be characterized by the unbalance parameters ϵ and Δ, where Δ is much less than unity and ϵ is small compared to π. The method described here enables rapid and distinct quantitative determination of ϵ and Δ. $S(t)$ is a switching function described over the time interval $(0, 2T)$ by

$$S(t) = \begin{cases} 0, & 0 \le t < T \\ 1, & T \le t < 2T \end{cases} \tag{4}$$

and repeating elsewhere at multiples of $2T$. It is beyond

the scope of this treatment to consider the spectral distribution of (2) and the details of the necessary band-limiting introduced by the components in the test arm. This treatment therefore assumes that the test-arm components have bandwidth sufficient such that the actual signals are adequately modeled by (2) even though in practice finite rise and fall times will necessarily be observed in the patterns.

C. The Detected Voltages

In terms of a radio demodulator implicitly modeled, the signal in the reference arm is the local oscillator which is combined in the hybrid with the (received) signal from the test arm. Since these signals have identical frequencies, the IF is zero and demodulation of the test-arm signal is achieved directly. The following derivation results in expressions for V^A and V^B in terms of the modulator amplitude and phase-unbalance parameters ϵ and Δ.

It can be shown that the output signals of the hybrid to the single-ended detectors A and B are, [4], [5]

$$V^A = V^{II} + V^I \tag{5a}$$

$$V^B = V^{II} - V^I. \tag{5b}$$

Substituting (1) and (2) into (5) and then into the transfer function for a square-law device,

$$V_{out}{}^\rho = a_1 V^\rho + a_2 (V^\rho)^2 +, \cdots, \qquad \rho = A, B \tag{6}$$

one obtains the following expression for the low-frequency or baseband component of the detected voltages:

$$V_{out}{}^A = (K_A/2)\{v^{I2} + v^{II2} + 2v^I v^{II} \cos[\theta(t) - \phi_0]\} \tag{7a}$$

$$V_{out}{}^B = (K_B/2)\{v^{I2} + v^{II2} - 2v^I v^{II} \cos[\theta(t) - \phi_0]\}. \tag{7b}$$

Substituting from (3) for $v^{II}(t)$ and assuming $v^{II} = v^I = v$ one obtains

$$V^{A'} = [1 \pm \Delta S(t)] \cos^2\left[\frac{\theta(t) - \phi_0}{2}\right] + \left[\frac{\Delta S(t)}{2}\right]^2 \tag{8a}$$

$$V^{B'} = [1 \pm \Delta S(t)] \sin^2\left[\frac{\theta(t) - \phi_0}{2}\right] + \left[\frac{\Delta S(t)}{2}\right]^2. \tag{8b}$$

Here the voltages $V^{A'}$ and $V^{B'}$ have been normalized by $2Kv^2$ to be unity in the balanced case, assuming that the detector constants have been effectively equalized so that $K_A = K_B = K$.

Of particular importance for the real-time display of the method described here is the complementary nature of (8). If one assumes that $\Delta = 0$ and the signals of the two arms are in phase so that $\theta(t) = \phi_0$, then $V^{B'}$ is nulled and all of the demodulated signal appears as $V^{A'}$. When the phase of the test signal changes by π, then the null and active voltages permute and the demodulated power appears as $V^{B'}$

III. THE PATTERNS

This section considers in detail the responses $V^{A'}$ and $V^{B'}$ for particular cases which are also of general significance. The test-arm conditions considered are as follows.

No Unbalance: $\Delta = 0$, $\epsilon = 0$.

Phase Unbalance: $\Delta = 0$, $\epsilon \neq 0$.

Amplitude Unbalance: $\Delta \neq 0$, $\epsilon = 0$.

For each of these test-arm conditions, four specific values of the reference-arm phase states are studied. It is convenient to group these phase states into two categories which are as follows.

Cophasal States: $\phi_0 = \theta_0, \theta_0 + \pi$.

Quadrature States: $\phi_0 = \theta_0 + \pi/2, \theta_0 - \pi/2$.

This leads to a total of six cases. Because of their simplicity, both the cophasal and quadrature reference states are considered as one case for the ideally balanced modulator. Therefore only five subsections actually follow. The first subsection considers this ideal modulator and the following ones analyze the four remaining cases. These four cases are of particular significance because they permit *any possible combination* of amplitude and phase unbalance in the test-arm modulator to be separately resolved and identified while that test-arm modulator is operating dynamically. This remarkable property is based on the fact that phase unbalance in the test-arm modulator is shown to uniquely induce a symmetric display pattern for both the quadrature and cophasal reference-arm states. Amplitude unbalance is shown to uniquely induce an asymmetric display pattern for both the quadrature and cophasal reference-arm states. Thus decomposing any observed pattern into symmetric and asymmetric components automatically resolves the phase and amplitude unbalance of the test-arm modulator. The ability to vary the reference-arm states at a rate commensurate with visual pattern recognition is of importance to this scheme since it will make the asymmetric component become evident as a crankshaft effect.

A. No Unbalance in Test Arm

Cophasal and Quadrature States in Reference Arm: In this case

$$\epsilon = 0 \qquad \Delta = 0.$$

First we consider the cophasal states. The normalized detected voltages $V^{A'}$ and $V^{B'}$, as computed from (8), are summarized in the table of Fig. 2 for all of four possible states. For example, when the reference arm is adjusted so that $\phi_0 = \theta_0$, $V^{A'}$ varies between unity and zero as denoted by states ① and ②. When the reference arm is changed so that $\phi_0 = \theta_0 + \pi$, then the complementary pattern denoted by ③ and ④ is obtained by $V^{A'}$. The four possible states for $V^{A'}$ are plotted as the display pattern at the bottom of the figure. On a real-time basis all four are not available simultaneously since this would require the reference arm to be in two states simultaneously. However, as noted earlier, $V^{B'}$ is the real-time complementary response of $V^{A'}$. $V^{B'}$ is simultaneously available from the hybrid with $V^{A'}$ and can be simultaneously displayed on a dual-trace oscilloscope with a common time base to give the pattern at the bottom of Fig. 2. All the

IDEAL CASE $\Delta=0$, $\epsilon=0$

STATE	TEST ARM - $\theta(t)$	REF. ARM - ϕ_0	$V^{A'}$	$V^{B'}$
①	θ_0	θ_0	1	0
②	$\theta_0+\pi$	θ_0	0	1
③	θ_0	$\theta_0+\pi$	0	1
④	$\theta_0+\pi$	$\theta_0+\pi$	1	0

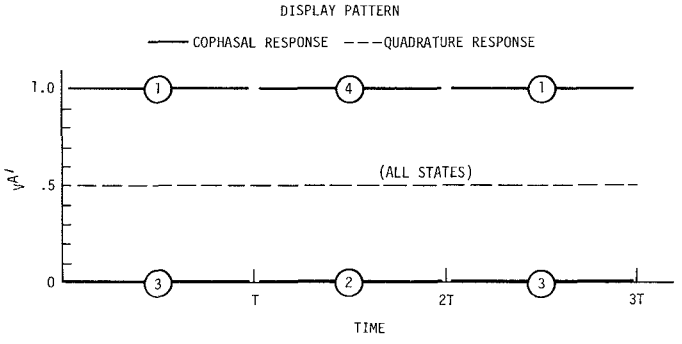

Fig. 2. Detected voltage versus time. Phase modulation periodic in $2T$. No unbalance in test arm; cophasal and quadrature states in reference arm.

PHASE UNBALANCE ONLY $\Delta=0$, $\epsilon\neq0$

STATE	TEST ARM - $\theta(t)$	REF ARM - ϕ_0	$V^{A'}$	$V^{B'}$
①	θ_0	θ_0	1	0
②	$\theta_0+\pi\pm\epsilon$	θ_0	$\sin^2\epsilon/2$	$\cos^2\epsilon/2$
③	θ_0	$\theta_0+\pi$	0	1
④	$\theta_0+\pi\pm\epsilon$	$\theta_0+\pi$	$\cos^2\epsilon/2$	$\sin^2\epsilon/2$

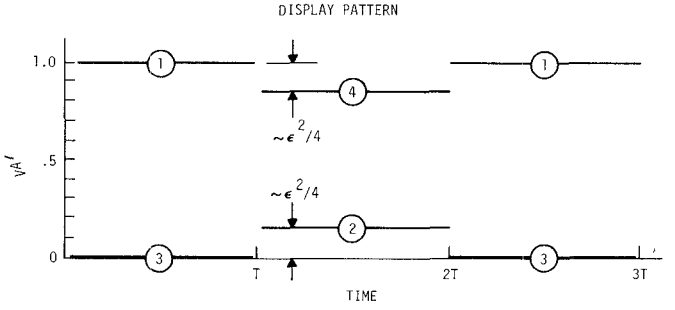

Fig. 3. Detected voltage versus time. Phase modulation periodic in $2T$. Phase unbalance in test arm; cophasal states in reference arm.

patterns subsequently described can be reproduced in this manner. For a perfectly balanced biphase, PSK modulator states ①, ④, and ②, ③ are perfectly aligned as shown in that figure.

For any arbitrary setting of the reference-arm phase ϕ_0 the values of $V^{A'}$ are determined from (8) which reduces to

$$V^{A'} = \cos^2\left(\frac{\theta(t) - \phi_0}{2}\right).$$

If the reference arm is set to be in phase quadrature ($\phi_0 = \theta_0 \pm \pi/2$) to the two states of the test arm, the responses for both $V^{A'}$ and $V^{B'}$ for all states will equal 0.5, as indicated by the dashed line.

It is generally true that the cophasal responses, as indicated by the heavy lines, are maximally divergent lines, while the quadrature response tends to coalesce to a single line about the mean value of the cophasal lines.

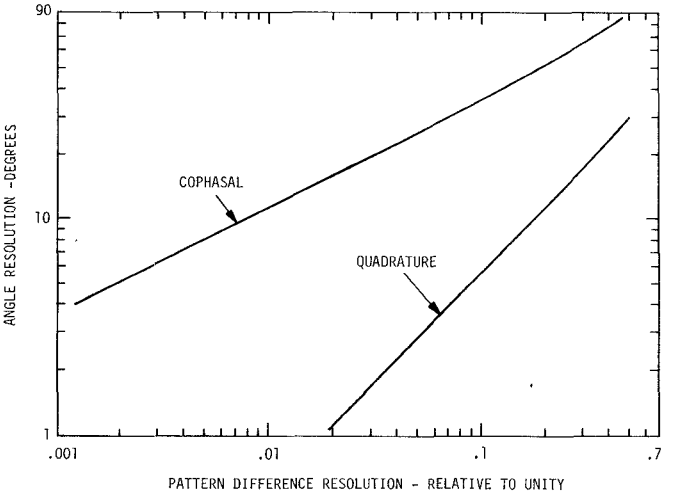

Fig. 4. Phase-bridge phase sensitivity. Angle resolution in degrees versus pattern-difference resolution (see Figs. 3 and 5) relative to unity.

B. Phase Unbalance in Test Arm

Cophasal States in Reference Arm: In this case

$$\Delta = 0 \qquad \epsilon \neq 0 \qquad \phi_0 = \theta_0, \theta_0 + \pi.$$

The normalized detected voltages $V^{A'}$ and $V^{B'}$ are summarized in the table given in Fig. 3 for the four possible cophasal states. The presence of phase unbalance in states ② and ④ causes them to "neck in" symmetrically about the average value line, as shown in the pattern at the bottom of the figure. The amount of necking is related to the phase unbalance ϵ by $\sin^2\epsilon/2$. Thus one can relate the resolution of states ① and ④ to the angle resolution by the use of Fig. 4. Because of the square-law relation, the cophasal response is not very sensitive since we must resolve ① and ④ to 0.01 to determine ϵ within $\pm$ 11.5°. It will be shown that the quadrature states produce much better sensitivity.

C. Phase Unbalance in Test Arm

Quadrature State in Reference Arm: In this case

$$\Delta = 0 \qquad \epsilon \neq 0 \qquad \phi_0 = \theta_0 + \pi/2, \theta_0 - \pi/2.$$

The normalized detected voltages $V^{A'}$ and $V^{B'}$ are summarized in the table given in Fig. 5 for the possible quadra-

PHASE UNBALANCE ONLY $\Delta=0$, $\epsilon \neq 0$

STATE	TEST ARM - $\theta(t)$	REF. ARM - ϕ_0	$V^{A'}$	$V^{B'}$
①	θ_0	$\theta_0+\pi/2$	$\frac{1}{2}$	$\frac{1}{2}$
②	$\theta_0+\pi\pm\epsilon$	$\theta_0+\pi/2$	$\frac{1}{2}(1\mp\sin\epsilon)$	$\frac{1}{2}(1\pm\sin\epsilon)$
③	θ_0	$\theta_0-\pi/2$	$\frac{1}{2}$	$\frac{1}{2}$
④	$\theta_0+\pi\pm\epsilon$	$\theta_0-\pi/2$	$\frac{1}{2}(1\pm\sin\epsilon)$	$\frac{1}{2}(1\mp\sin\epsilon)$

DISPLAY PATTERN

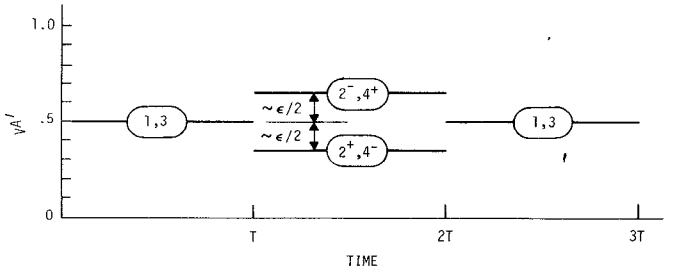

Fig. 5. Detected voltage versus time. Phase modulation periodic in $2T$. Phase unbalance in test arm; quadrature states in reference arm.

AMPLITUDE UNBALANCE ONLY $\Delta\neq 0$, $\epsilon=0$

STATE	TEST ARM v^{II}	TEST ARM $\theta(t)$	REF. ARM ϕ_0	$V^{A'}$	$V^{B'}$
①	1	θ_0	θ_0	1	0
②	$1\pm\Delta$	$\theta_0+\pi$	θ_0	$(\Delta/2)^2$	$(1\pm\Delta/2)^2$
③	1	θ_0	$\theta_0+\pi$	0	1
④	$1\pm\Delta$	$\theta_0+\pi$	$\theta_0+\pi$	$(1\pm\Delta/2)^2$	$(\Delta/2)^2$

DISPLAY PATTERN

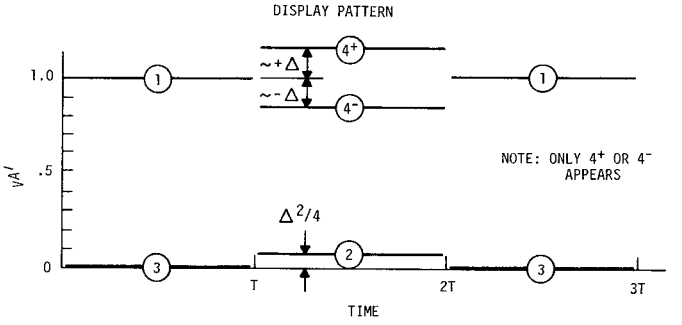

Fig. 6. Detected voltage versus time. Phase modulation periodic in $2T$. Amplitude unbalance in test arm; cophasal states in reference arm.

ture states. It is seen that states ① and ③ coalesce to a common line of normalized value 0.5. States ② and ④ differ by $\sin\epsilon \approx \epsilon$. Since for cophasal reference states this unbalance term was $\epsilon^2/4$, the quadrature sensitivity is more than one order of magnitude greater than the cophasal sensitivity as shown in Fig. 4. For example, to achieve the $\pm$ 11.5° angle resolution, one need only resolve quadrature states ②⊖ and ④⊖ or ②⊕ and ④⊕ to within 0.2. This is twenty times less stringent than the cophasal case and is a more realistic quantity for graphical display resolution. It is also important to note that the phase unbalance results in a pattern which is symmetric about the median value of 0.5. The pattern of Section III-B for cophasal reference states also had this symmetry.

D. Amplitude Unbalance in Test Arm

Cophasal States in Reference Arm: In this case

$$\Delta \neq 0 \qquad \epsilon = 0 \qquad \phi_0 = \theta_0, \theta_0 + \pi.$$

The normalized detected voltages $V^{A'}$ and $V^{B'}$ are summarized in the table of Fig. 6 for the four states. The presence of the amplitude unbalance $\pm\Delta$ causes ② to be offset from zero by $\Delta^2/4$ while ④ is offset from unity by either $+\Delta$ or $-\Delta$. As noted in the figure, only one of these appears, so the net pattern is asymmetrical about the center axis. Thus as the phase of the reference arm is varied between states, an asymmetrical crankshaft effect becomes evident. This easily distinguishes amplitude unbalance from the phase-unbalance patterns considered in Sections III-B and III-C.

It is also significant to note that the amplitude unbalance is linear in Δ. Thus for cophasal states the sensitivity to amplitude unbalance is considerably greater than phase unbalance.

E. Amplitude Unbalance in Test Arm

Quadrature States in Reference Arm: In this case

$$\Delta \neq 0 \quad \epsilon = 0 \quad \phi_0 = \theta_0 + \pi/2, \theta_0 - \pi/2.$$

The normalized voltages $V^{A'}$ and $V^{B'}$ are summarized in Fig. 7. States ① and ③ coalesce to a common value of 0.5. The presence of an amplitude unbalance $+\Delta$ causes both ② and ④ to be offset by $\Delta/2 + \Delta^2/4$ while $-\Delta$ causes both ② and ④ to be offset by $-\Delta/2 + \Delta^2/4$. Thus the pattern is asymmetric since the sign of the deviation is always determined by the sign of Δ and not the state of the reference arm. The sensitivity here is approximately half that for the cophasal states.

IV. SUMMARY

1) The technique proposed herein for characterizing the RF portion of the radio can be interpreted as a receiver with zero IF that yields demodulated data directly.

2) The use of a hybrid combiner and an appropriate phase shifter permit a convenient dynamic real-time display of the dynamic amplitude and phase unbalance on a dual-trace oscilloscope.

3) The scheme assumed that the detectors were representable and operated as square-law devices.

AMPLITUDE UNBALANCE ONLY $\Delta \neq 0$, $\epsilon = 0$

STATE	TEST ARM v^{II}	TEST ARM $\theta(t)$	REF. ARM ϕ_0	$v^{A'}$	$v^{B'}$
①	1	θ_0	$\theta_0+\pi/2$	$\frac{1}{2}$	$\frac{1}{2}$
②	$1\pm\Delta$	$\theta_0+\pi$	$\theta_0+\pi/2$	$\frac{1}{2}(1\pm\Delta)+\frac{\Delta^2}{4}$	$\frac{1}{2}(1\pm\Delta)+\frac{\Delta^2}{4}$
③	1	θ_0	$\theta_0-\pi/2$	$\frac{1}{2}$	$\frac{1}{2}$
④	$1\pm\Delta$	$\theta_0+\pi$	$\theta_0-\pi/2$	$\frac{1}{2}(1\pm\Delta)+\frac{\Delta^2}{4}$	$\frac{1}{2}(1\pm\Delta)+\frac{\Delta^2}{4}$

DISPLAY PATTERN

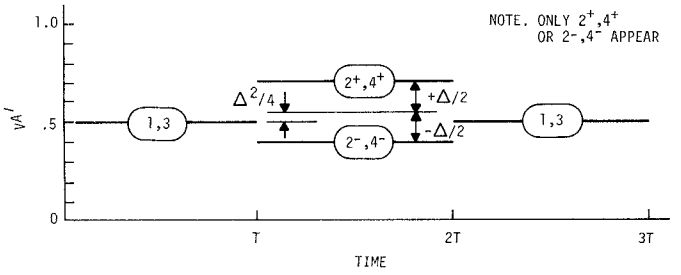

Fig. 7. Detected voltage versus time. Phase modulation periodic in $2T$. Amplitude unbalance in test arm; quadrature states in reference arm.

4) Two sets of reference-arm states prove to be particularly useful for analyzing a biphase PSK modulator, viz., cophasal and quadrature. With these reference-arm conditions it is shown that phase unbalance provides a symmetric pattern about the central axis while amplitude unbalance is asymmetric, readily permitting distinction.

5) In the cophasal states, small phase deviations produce only second-order errors and thus are not particularly sensitive.

6) In the quadrature states, small phase deviations produce a linear error term. Thus, the sensitivity is at least one order of magnitude greater for small deviations. The amplitude-unbalance error is still linear, but the error term is half that for the cophasal states.

7) The essential feature of the technique described herein is that it permits a static or very slowly varying phase shifter to dynamically calibrate a second phase shifter (i.e., a PSK modulator). Furthermore, if the phase shifter is continuously variable it is not essential that it be calibrated.

ACKNOWLEDGMENT

The author wishes to thank R. F. Hazel for his prior experimental work and also for his reading and criticism of the manuscript.

REFERENCES

[1] D. M. Kerns and R. W. Beatty, *Basic Theory of Waveguide Junctions and Introductory Microwave Network Analysis.* New York: Pergamon, 1967.
[2] J. D. Dyson, "The measurement of phase at UHF and microwave frequencies," *IEEE Trans. Microwave Theory Tech.*, vol. MTT-14, pp. 410–423, Sept. 1966.
[3] R. V. Garver, D. E. Bergfried, S. J. Raff, and B. O. Weinschel, "Errors in S_{11} measurements due to the residual standing-wave ratio of the measuring equipment," *IEEE Trans. Microwave Theory Tech. (Special Issue on Automated Microwave Measurements)*, vol. MTT-20, pp. 61–69, Jan. 1972.
[4] C. G. Montgomery *et al.*, *Principles of Microwave Circuits* (M.I.T. Radiation Laboratory Series). New York: McGraw-Hill, 1948.
[5] J. L. Altman, *Microwave Circuits.* Princeton, N. J.: Van Nostrand, 1964.